# Electronic Supplementary Information

## How hexafluoroisopropanol solvent promotes Diels-Alder cycloadditions: ab initio metadynamics simulations

Xia Zhao,[a] Xinmin Hu,[a] Xiangying Lv,[a] Yan-Bo Wu,[b] Yuxiang Bu[a] and Gang Lu*[a]

[a] School of Chemistry and Chemical Engineering, Key Laboratory of Colloid and Interface Chemistry, Ministry of Education, Shandong University, Jinan, Shandong 250100, China

[b] Key Lab for Materials of Energy Conversion and Storage of Shanxi Province and Key Lab of Chemical Biology and Molecular Engineering of Ministry of Education, Institute of Molecular Science, Shanxi University, Taiyuan, Shanxi 030006, China

Corresponding Author: ganglu@sdu.edu.cn

## Table of Contents

**Computational Details**

The solvent box was modeled using a cubic periodic cell of 14 × 14 × 14 Å$^3$. This dimension ensures the distances between the solutes in two adjacent cells are longer than 6 Å, which can avoid interactions with neighboring solutes. To correspond with the densities of pure solvents (1.605 g/cm$^3$ for HFIP and 0.870 g/cm$^3$ for toluene), the periodic cells of HFIP and toluene boxes contain 15 HFIP and 14 toluene molecules in the presence of substrate, respectively. All AIMD and metadynamics simulations were performed using the Quickstep module of CP2K package.[1] DFT calculations with the PBE functional[2] and the hybrid Gaussian basis set (DZVP)/plane-wave pseudopotentials (GTH)[3] were carried out to estimate atomic forces for all atoms. The Grimme D3 dispersion corrections were used to describe dispersion interactions.[4] The dispersion-corrected GGA functional PBE-D3 has been previously utilized to sufficiently describe the dynamical properties of various chemical transformations under periodic explicit solvent boxes.[5] The cutoff level of plane-wave basis set was set at 280 Ry. Higher values of cutoff show comparable relative activation free energies (see details in Table S1). The BOMD simulations[6] with a time step of 0.5 fs were performed in the NVT ensemble and the temperature was controlled by the Nosé-Hoover thermostat.[7]

Each system was equilibrated via short AIMD simulations (ca. 3~5 ps) at the experimental temperature (303 K) to generate the initial configurations of solvents and solutes for the subsequent metadynamics simulations. The coordination numbers (CNs), indicated by $CN = [1 - (d/d_0)^6]/[1 - (d/d_0)^{12})]$, were used as collective variables. In the equation of CNs, $d$ is the distance between two atoms and $d_0$ is the predefined reference distance. At the same temperatures with short AIMD simulations, well-tempered metadynamics simulations,[8] which can avoid the fluctuations of free energy surfaces and provide exact estimations, were carried out to construct free energy surfaces of Diels-Alder cycloadditions. Gaussian potential hills with an initial height of 0.6 kcal/mol and a width of 0.1 were added every 50 steps along the two collective variables. In the well-tempered metadynamics simulations, the $\Delta T$ parameter, which controls how quickly the Gaussian height is decreased, was set to 35~40 times of the simulation temperature. After the convergence of simulations (see details in Fig. S1), the free energy surfaces and the minimum energy paths were obtained by using the metadynminer code developed by Spiwok.[9]

Energy decomposition analysis (EDA) calculations at the PBE-D3/def2-TZVP level of theory were performed by using the second-generation EDA based on absolutely localized orbitals (ALMO-EDA2) implemented in Q-Chem 5.2.[10] The orbital coefficients were computed at PBE-D3/def2-TZVP by using Gaussian 16.[11] The geometries were visualized by using the VMD software.[12]

**Criteria for Convergence of Well-Tempered Metadynamics Simulations**

The time to stop simulations is important for the accuracy of free energy surfaces (FESs). We here use two criteria for the convergence of FESs: 1) in the well-tempered metadynamics simulations, the Gaussian height should be decreased over time and reach a small value (ca. < 0.1 kcal/mol); 2) the free energy profiles do not change anymore over time. Taking the simulation of Diels-Alder reaction in HFIP as an example, the Gaussian height is decreased to 0.04 kcal/mol after the 83 ps simulation (Fig. S1). While there are significant changes in free energies along the two CVs (d1 and d2) at the early stage of simulations (before 60 ps), the free energies obtained at 83 ps are nearly unchanged for both CVs (Fig. S1). Thus, the well-tempered metadynamics simulation is converged and the free energy surface is accurately constructed.

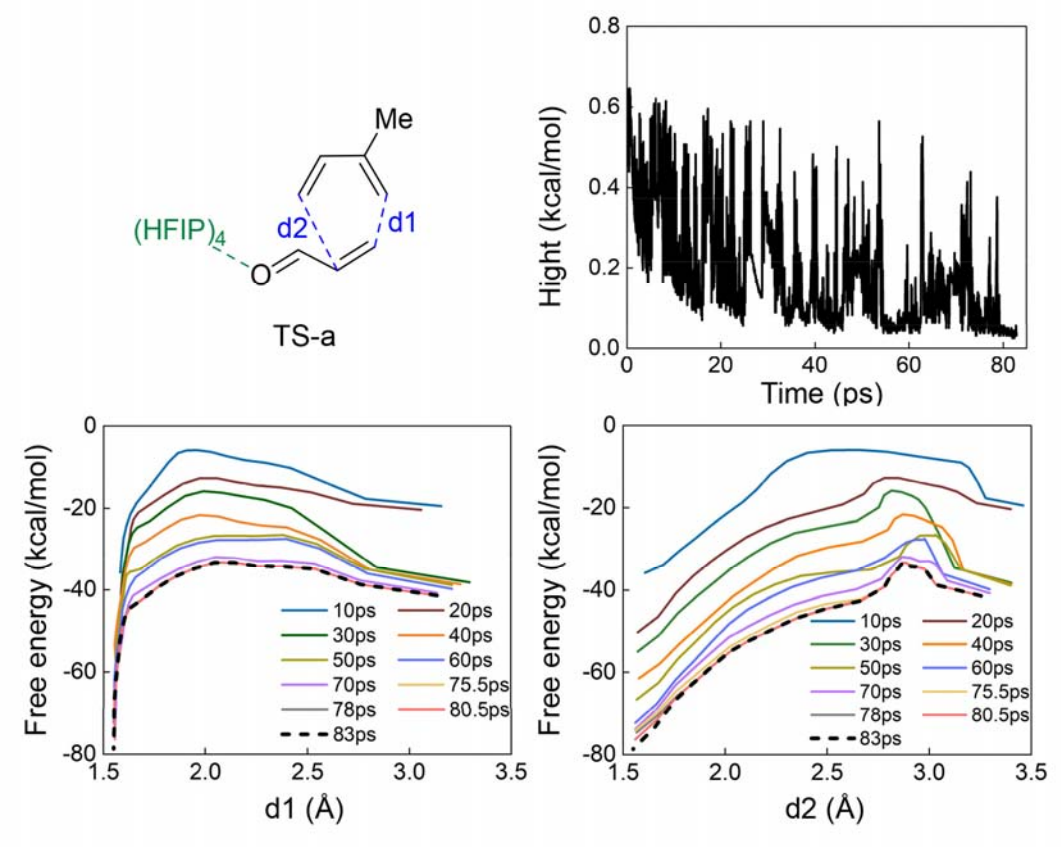


**Fig. S1** Changes of Gaussian heights and free energies during simulations.

**Effect of Plane-Wave Cutoff Values on Activation Free Energies**

Since the plane-wave basis set expended at different cutoff values could affect the energetics, we thus studied the effect of cutoff on the activation free energies for the reactions in HFIP and toluene (e.g., **TS-a** and **TS-b**). As shown in Table S1, although the absolute values of activation free energies are different when employing 280, 400 and 500 Ry cutoff, the trend between **TS-a** and **TS-b** is not changed. This indicates that the superior reactivity with HFIP is not affected by the choice of cutoff. Because of the time-consuming simulations with higher cutoff values, the activation free energies computed at 280 Ry cutoff are reported in this work.

**Table S1 Activation free energies at different cutoff values**

| **Transition states** | **Plane-wave basis set cutoff** | | |
|---|---|---|---|
| | 280 Ry | 400 Ry | 500 Ry |
| **TS-a** $\Delta G^{\ddagger}_{\mathrm{HFIP}}$ (kcal/mol) | 8.2 | 8.7 | 7.1 |
| **TS-b** $\Delta G^{\ddagger}_{\mathrm{Toluene}}$ (kcal/mol) | 15.5 | 20.6 | 22.7 |

**H-Bonding Interactions of HFIP Molecules**

To study the H-bonding interactions of HFIP molecules, we built a pure solvent box containing 46 HFIP molecules and performed 6 ps AIMD simulations. The results show that both O–H···O and O–H···F interactions can be found (**A** and **B**, Fig. S2). The HFIP molecule can simultaneously serve as the H-bonding donor and acceptor (**C** and **D**). These solvent-solvent interactions involve the dimer, trimer and tetramer of HFIP molecules. It can be expected that the microenvironments of HFIP are dynamically changed during the reaction process, and exert influence on the solvent-solute interactions.

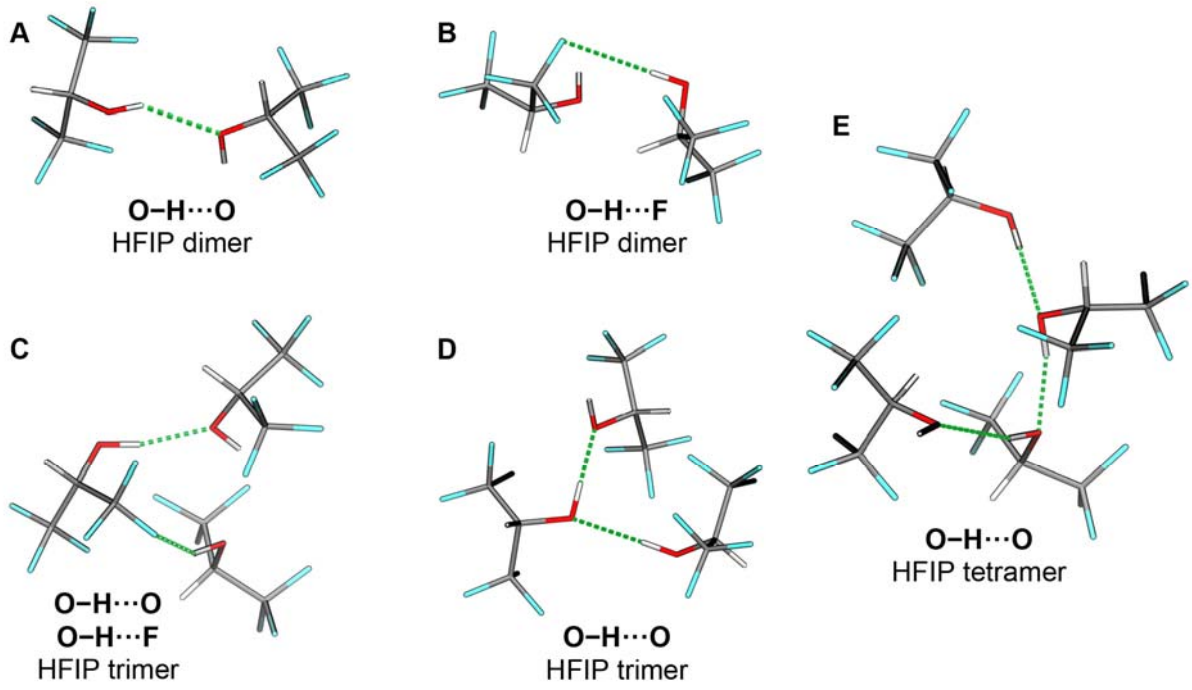


**Fig. S2** Complex H-bonding interactions of HFIP molecules.

**Representative Structure Snapshots of Reactants and Products**

Based on the obtained MEP of FESs, the snapshots of corresponding reactants (**Re-a**~**Re-d**) and products (**Pr-a**~**Pr-d**) can be extracted from the trajectories of metadynamics simulations (Fig. S3).

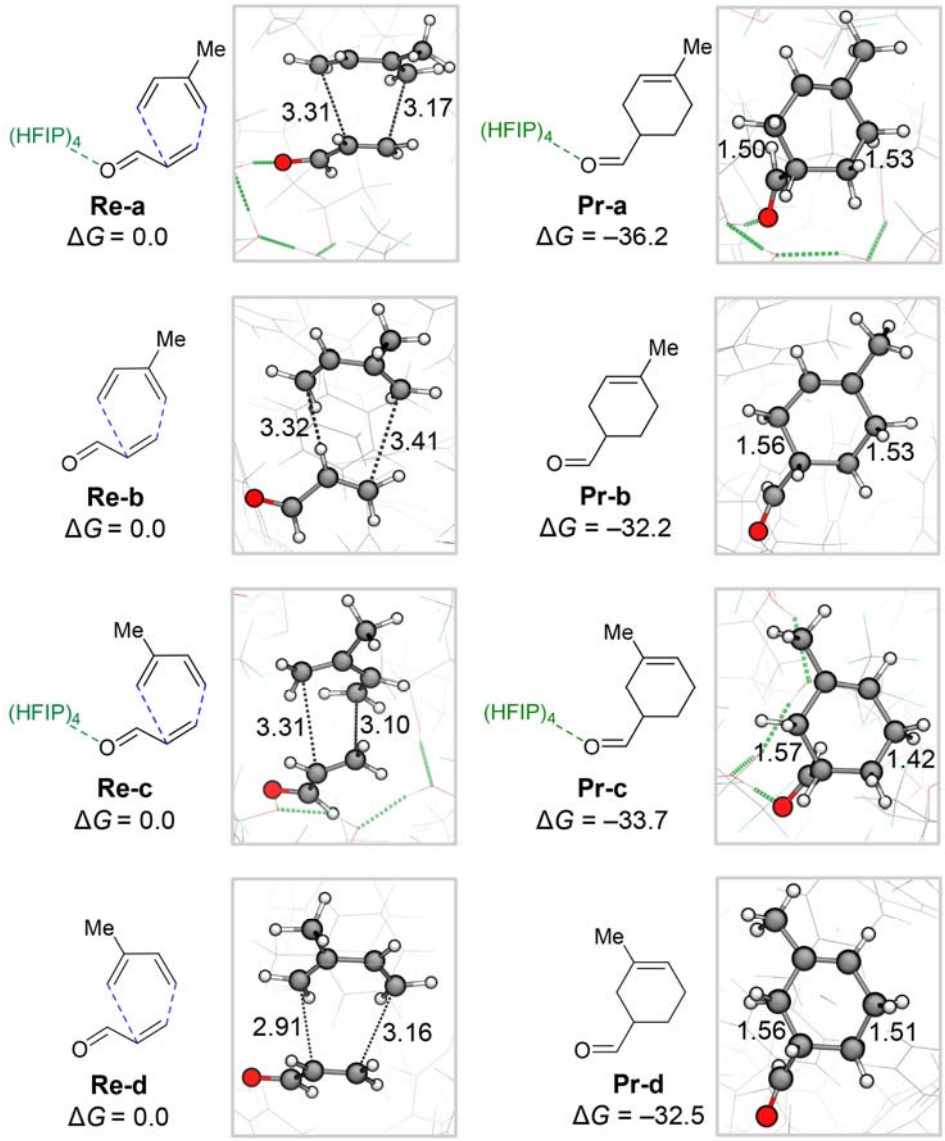


**Fig. S3** The snapshots of reactants and products of Diels-Alder cycloadditions in HFIP and toluene solvents. Energies and key bond distances are shown in kcal/mol and Å, respectively.

## EDA Results along MEP

**Table S2 EDA energy terms of TS-a along MEP**

| TS-a (HFIP, para-selective) | | | | | |
|---|---|---|---|---|---|
| **Distance d1 (Å)** | **$\Delta E_{elstat}$** | **$\Delta E_{Pauli}$** | **$\Delta E_{disp}$** | **$\Delta E_{pol}$** | **$\Delta E_{ct}$** |
| 2.53 | -13.17 | 30.73 | -11.73 | -2.23 | -15.69 |
| 2.38 | -20.47 | 50.45 | -14.26 | -3.01 | -22.98 |
| 2.29 | -22.42 | 52.69 | -14.55 | -3.63 | -26.94 |
| 2.15 | -31.36 | 77.77 | -15.75 | -4.61 | -31.95 |
| 2.05 (TS) | -38.26 | 94.75 | -17.95 | -6.61 | -47.27 |
| 1.96 | -47.12 | 113.24 | -18.92 | -9.70 | -58.62 |
| 1.87 | -66.07 | 149.77 | -23.02 | -17.49 | -85.42 |
| 1.79 | -75.96 | 171.96 | -22.87 | -25.29 | -102.36 |
| 1.71 | -90.88 | 205.85 | -23.33 | -38.70 | -123.49 |
| 1.67 | -103.38 | 246.17 | -27.60 | -43.66 | -121.33 |
| 1.63 | -119.52 | 270.54 | -28.14 | -66.14 | -145.82 |
| 1.6 | -131.83 | 302.85 | -30.42 | -72.81 | -146.86 |

**Table S3 EDA energy terms of TS-b along MEP**

| TS-b (toluene, para-selective) | | | | | |
|---|---|---|---|---|---|
| **Distance d1 (Å)** | **$\Delta E_{elstat}$** | **$\Delta E_{Pauli}$** | **$\Delta E_{disp}$** | **$\Delta E_{pol}$** | **$\Delta E_{ct}$** |
| 2.56 | -19.49 | 51.34 | -22.70 | -2.10 | -11.36 |
| 2.43 | -23.76 | 60.13 | -22.72 | -2.60 | -17.52 |
| 2.29 | -32.26 | 82.83 | -25.86 | -3.80 | -23.95 |
| 2.2 | -34.13 | 87.03 | -25.21 | -4.49 | -30.83 |
| 2.10 (TS) | -41.91 | 102.30 | -26.86 | -6.26 | -44.08 |
| 2.03 | -50.17 | 119.15 | -30.31 | -30.31 | -52.18 |
| 1.95 | -69.42 | 163.30 | -30.87 | -15.41 | -81.35 |
| 1.89 | -70.44 | 168.68 | -28.08 | -16.86 | -94.92 |
| 1.84 | -93.06 | 222.74 | -37.35 | -27.64 | -103.25 |
| 1.79 | -106.85 | 239.53 | -34.39 | -41.12 | -134.58 |
| 1.74 | -114.61 | 257.70 | -35.85 | -44.34 | -137.77 |
| 1.66 | -126.26 | 267.54 | -33.20 | -64.80 | -157.45 |

**Table S4 EDA energy terms of TS-c along MEP**

| TS-c (HFIP, meta-selective) | | | | | |
|---|---|---|---|---|---|
| **Distance d1(Å)** | $\Delta E_{elstat}$ | $\Delta E_{Pauli}$ | $\Delta E_{disp}$ | $\Delta E_{pol}$ | $\Delta E_{ct}$ |
| 2.54 | -16.07 | 38.89 | -13.30 | -2.17 | -12.85 |
| 2.38 | -21.00 | 50.16 | -14.69 | -2.94 | -21.61 |
| 2.27 | -26.14 | 64.21 | -16.07 | -3.59 | -26.19 |
| 2.16 | -32.95 | 79.16 | -17.03 | -5.22 | -36.39 |
| 2.06 (TS) | -39.44 | 97.22 | -18.66 | -6.95 | -48.74 |
| 2.01 | -46.02 | 111.03 | -19.77 | -9.16 | -56.92 |
| 1.92 | -64.79 | 157.75 | -26.22 | -15.02 | -75.36 |
| 1.88 | -73.71 | 166.28 | -24.85 | -21.91 | -103.25 |
| 1.84 | -78.91 | 184.32 | -26.48 | -24.11 | -104.41 |
| 1.79 | -93.68 | 215.53 | -30.19 | -35.01 | -125.51 |
| 1.71 | -107.89 | 238.99 | -29.44 | -49.86 | -146.26 |
| 1.64 | -134.04 | 297.33 | -31.96 | -74.00 | -163.98 |

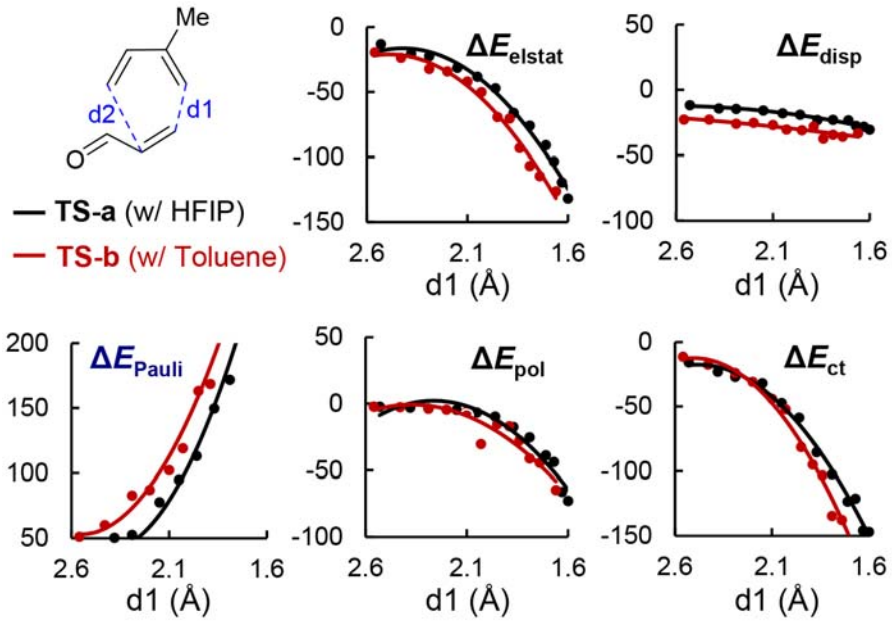


**Fig. S4** Comparison of EDA results between **TS-a** and **TS-b** along their MEPs. Energies are given in kcal/mol.

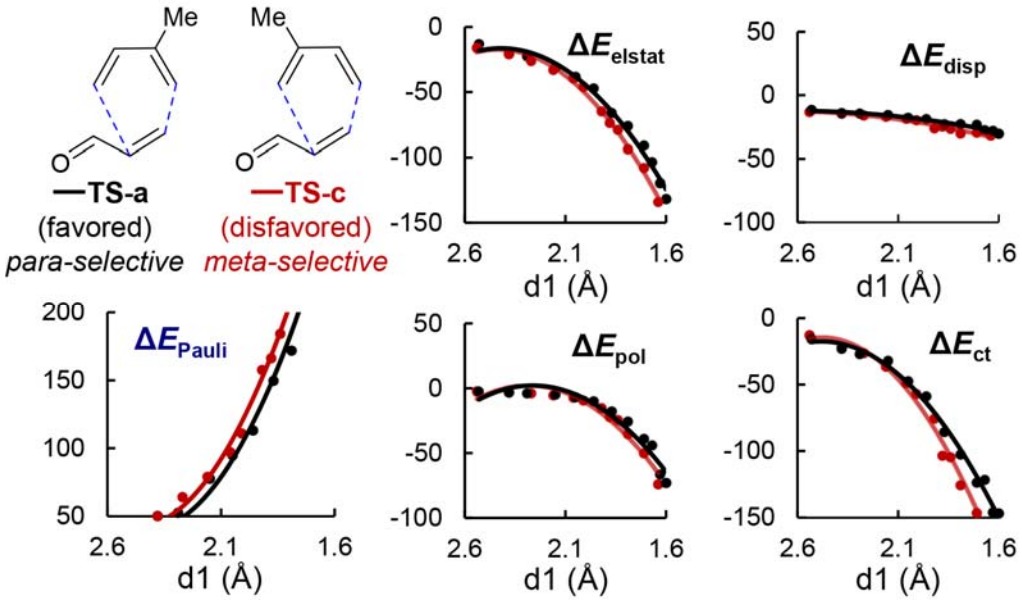


**Fig. S5** Comparison of EDA results between **TS-a** and **TS-c** along their MEPs. Energies are given in kcal/mol.

**Interactions between HFIP and the Methyl Group during Simulations**

Based on the 5 ps AIMD simulations of **TS-a** and **TS-c**, we found that three HFIP molecules can aggregate around the methyl group of isoprene via the C–H···F interactions. The distances of C–H···F hydrogen bonds (H-bond 1~3) between the methyl group and the first HFIP molecule in **TS-a** and **TS-c** are given in Fig. S6. The second and third HFIP molecules interact with the first one via O–H···O hydrogen bonds (H-bond 5 and 6). Because the interactions between HFIP aggregates and the methyl group are stable during the simulations, the H-bonding network around aldehyde in disfavored **TS-c** can be weakened due to steric effects.

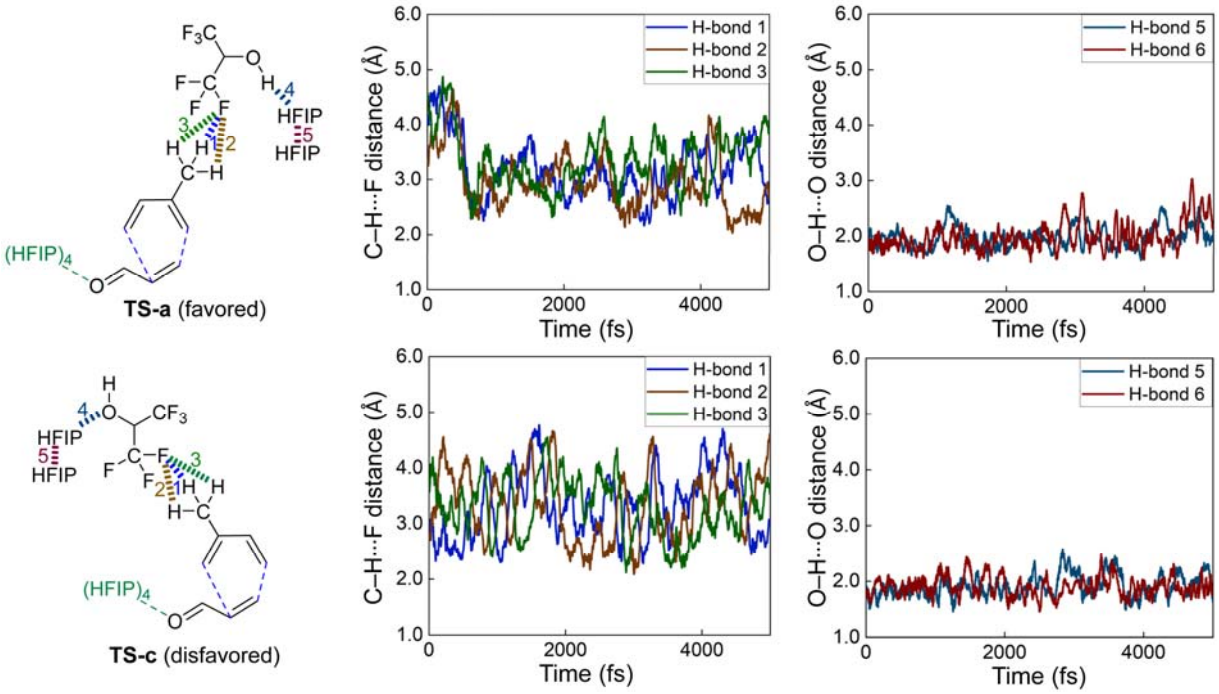


**Fig. S6** The dynamic feature of H-bonding networks.

**Activation Barriers with Implicit Solvent Model**

We further calculated the Diels-Alder transition states with the implicit solvent model (e.g., SMD) at PBE-D3/def2-TZVP (SMD)//PBE-D3/def2-SVP (SMD) level of theory. The computed barrier difference between **TS-a1** with HFIP and **TS-b1** with toluene is 2.6 kcal/mol, which is not enough to account for the significant difference in reaction rate (ca. 1128 times faster in HFIP than in toluene). In contrast, under explicit solvent environments, the barrier difference between **TS-a** (in HFIP) and **TS-b** (in toluene) is enlarged to 7.3 kcal/mol. This emphasizes that explicit solvent molecules can exert great influence on the reactivity of this Diels-Alder reaction.


**TS-a1**
$\Delta G^{\ddagger}$ = 16.1 kcal/mol
SMD model with HFIP

**TS-b1**
$\Delta G^{\ddagger}$ = 18.7 kcal/mol
SMD model with toluene

**Fig. S7** Computed barriers of Diels-Alder transition states with the implicit solvent model.

**Example of CP2K Input File for Well-Tempered Metadynamics Simulations**

```
&GLOBAL
  RUN_TYPE MD
  PROJECT wtmetad-HFIP
&END GLOBAL
&FORCE_EVAL
  METHOD Quickstep
  STRESS_TENSOR ANALYTICAL
  &DFT
    BASIS_SET_FILE_NAME BASIS_MOLOPT
    POTENTIAL_FILE_NAME GTH_POTENTIALS
    LSD
    CHARGE 0
    MULTIPLICITY 1
    &MGRID
      CUTOFF 280
      NGRIDS 5
    &END MGRID
    &QS
      METHOD GPW
      EPS_DEFAULT 1.0E-10
      EXTRAPOLATION ASPC
    &END QS
    &POISSON
      PERIODIC XYZ
      POISSON_SOLVER PERIODIC
    &END POISSON
    &SCF
      SCF_GUESS ATOMIC
      EPS_SCF 1.0E-5
      MAX_SCF 50
      &OUTER_SCF
        EPS_SCF 1.0E-5
        MAX_SCF 50
      &END OUTER_SCF
      &OT
        MINIMIZER DIIS
        PRECONDITIONER FULL_ALL
        ENERGY_GAP 0.001
      &END OT
    &END SCF
    &XC
      &XC_FUNCTIONAL
        &PBE
          PARAMETRIZATION ORIG
        &END PBE
      &END XC_FUNCTIONAL
      &VDW_POTENTIAL
        POTENTIAL_TYPE PAIR_POTENTIAL
        &PAIR_POTENTIAL
          PARAMETER_FILE_NAME ./dftd3.dat
          TYPE DFTD3
          REFERENCE_FUNCTIONAL PBE
          R_CUTOFF 16
        &END PAIR_POTENTIAL
      &END VDW_POTENTIAL
```

```
    &END XC
  &END DFT
  &SUBSYS
    &CELL
      ABC 14 14 14
    &END CELL
    &TOPOLOGY
      COORD_FILE_NAME 1.xyz
      COORD_FILE_FORMAT XYZ
    &END TOPOLOGY
    &KIND H
      ELEMENT H
      BASIS_SET DZVP-MOLOPT-SR-GTH
      POTENTIAL GTH-PBE-q1
    &END
    &KIND O
      ELEMENT O
      BASIS_SET DZVP-MOLOPT-SR-GTH
      POTENTIAL GTH-PBE-q6
    &END
    &KIND C
      ELEMENT C
      BASIS_SET DZVP-MOLOPT-SR-GTH
      POTENTIAL GTH-PBE-q4
    &END
    &KIND F
      ELEMENT F
      BASIS_SET DZVP-MOLOPT-SR-GTH
      POTENTIAL GTH-PBE-q7
    &END
    &COLVAR
      &COORDINATION
        ATOMS_FROM 6
        ATOMS_TO 12
        R0 [angstrom] 2.0
      &END COORDINATION
    &END COLVAR
    &COLVAR
      &COORDINATION
        ATOMS_FROM 4
        ATOMS_TO 9
        R0 [angstrom] 2.0
      &END COORDINATION
    &END COLVAR
  &END SUBSYS
&END FORCE_EVAL
&MOTION
  &MD
    ENSEMBLE NVT
    TEMPERATURE 303
    TIMESTEP 0.5
    STEPS 100000
    &THERMOSTAT
      TYPE NOSE
      &NOSE
        LENGTH 3
        YOSHIDA 3
```

```
        TIMECON 1000.0
        MTS 2
      &END NOSE
    &END THERMOSTAT
  &END MD
  &FREE_ENERGY
    &METADYN
      DO_HILLS
      NT_HILLS 50
      WW 1.0e-3
      WELL_TEMPERED
      DELTA_T 10605
      &METAVAR
        SCALE 0.1
        COLVAR 1
        &WALL
          POSITION 0.015
          TYPE REFLECTIVE
          &REFLECTIVE
            DIRECTION WALL_MINUS
          &END REFLECTIVE
        &END WALL
      &END METAVAR
      &METAVAR
        SCALE 0.1
        COLVAR 2
     &WALL
          POSITION 0.015
          TYPE REFLECTIVE
           &REFLECTIVE
             DIRECTION WALL_MINUS
           &END REFLECTIVE
        &END WALL
      &END METAVAR
      &PRINT
        &COLVAR
          COMMON_ITERATION_LEVELS 3
        &END COLVAR
        &HILLS
          COMMON_ITERATION_LEVELS 3
        &END HILLS
      &END PRINT
    &END METADYN
  &END FREE_ENERGY
&END MOTION
```

## References


1 (a) J. VandeVondele, M. Krack, F. Mohamed, M. Parrinello, T. Chassaing and J. Hutter, *Comput. Phys. Commun.,* 2005, **167**, 103-128; (b) T. D. Kühne, M. Iannuzzi, M. Del Ben, V. V. Rybkin, P. Seewald, F. Stein, T. Laino, R. Z. Khaliullin, O. Schütt, F. Schiffmann, D. Golze, J. Wilhelm, S. Chulkov, M. H. Bani-Hashemian, V. Weber, U. Borštnik, M. Taillefumier, A. S. Jakobovits, A. Lazzaro, H. Pabst, T. Müller, R. Schade, M. Guidon, S. Andermatt, N. Holmberg, G. K. Schenter, A. Hehn, A. Bussy, F. Belleflamme, G. Tabacchi, A. Glöß, M. Lass, I. Bethune, C. J. Mundy, C. Plessl, M. Watkins, J. VandeVondele, M. Krack and J. Hutter, *J. Chem. Phys.,* 2020, **152**, 194103; (c) CP2K Open Source Molecular Dynamics. https://www.cp2k.org/quickstep.

2 J. P. Perdew, K. Burke and M. Ernzerhof, *Phys. Rev. Lett.,* 1996, **77**, 3865-3868.

3 (a) B. G. Lippert, J. H. Parrinello and Michele, *Mol. Phys.,* 1997, **92**, 477-488; (b) J. VandeVondele and J. Hutter, *J. Chem. Phys.,* 2007, **127**, 114105; (c) M. Krack, *Theor. Chem. Acc.,* 2005, **114**, 145-152.

4 S. Grimme, J. Antony, S. Ehrlich and H. Krieg, *J. Chem. Phys.,* 2010, **132**, 154104.

5 (a) R. M. Peltzer, O. Eisenstein, A. Nova and M. Cascella, *J. Phys. Chem. B,* 2017, **121**, 4226-4237; (b) A. C. Castro, D. Balcells, M. Repisky, T. Helgaker and M. Cascella, *Inorg. Chem.,* 2020, **59**, 17509-17518; (c) R. M. Peltzer, J. Gauss, O. Eisenstein and M. Cascella, *J. Am. Chem. Soc.,* 2020, **142**, 2984-2994; (d) Y. Fu, L. Bernasconi and P. Liu, *J. Am. Chem. Soc.,* 2021, **143**, 1577-1589; (e) F. Shao, J. K. Wong, Q. H. Low, M. Iannuzzi, J. Li and J. Lan, *Proc. Natl. Acad. Sci.,* 2022, **119**, e2118166119; (f) J.-W. Chen, Z. Zhang, H.-M. Yan, G.-J. Xia, H. Cao and Y.-G. Wang, *Nat. Commun.,* 2022, **13**, 1734.

6 D. Marx, J. Hutter, *Ab Initio Molecular Dynamics: Basic Theory and Advanced Methods,* Cambridge University Press, Cambridge, 2009.

7 (a) S. Nosé, *J. Chem. Phys.,* 1984, **81**, 511-519; (b) W. G. Hoover, *Phys. Rev.* A, 1985, **31**, 1695-1697; (c) G. J. Martyna, M. L. Klein and M. Tuckerman, *J. Chem. Phys.,* 1992, **97**, 2635-2643.

8 A. Barducci, G. Bussi and M. Parrinello, *Phys. Rev. Lett.,* 2008, **100**, 020603.

9 P. Hošek and V. Spiwok, *Comput. Phys. Commun.,* 2016, **198**, 222-229.

10 Y. Shao, Z. Gan, E. Epifanovsky, A. T. B. Gilbert, J. Kussmann, A. W. Lange, D. Ghosh, M. Goldey, P. R. Horn, I. Kaliman, R. Z. Khaliullin, T. Kuś, E. I. Proynov, M. A. Rohrdanz, R. P. Steele, E. J. Sundstrom, P. M. Zimmerman, D. Zuev, B. Albrecht, E. Alguire, E. Berquist, K. Brandhorst, D. Casanova, Y. Chen, S. H. Chien, D. L. Crittenden, M. Diedenhofen, R. A. Distasio, A. D. Dutoi, R. G. Edgar, S. Fatehi, L. FustiMolnar, A. Ghysels, A. Golubeva-Zadorozhnaya, J. Gomes, M. W. D. Hanson-Heine, P. H. P. Harbach, E. G. Hohenstein, Z. C. Holden, T. Jagau, H. Ji, B. Kaduk, K. Khistyaev, P. Klunzinger, T. Kowalczyk, C. M. Krauter, K. V. Lawler, S. V. Levchenko, F. Liu, R. C. Lochan, S. Mao, A. V. Marenich, S. A. Maurer, C. M. Oana, R. OlivaresAmaya, D. P. O'Neill, T. M. Perrine, R. Peverati, A. Prociuk, D. R. Rehn, N. J. Russ, S. M. Sharada, S. Sharma, A. Sodt, T. Stein, D. Stück, Y. Su, T. Tsuchimochi, L. Vogt, O. Vydrov, M. A. Watson, J. Wenzel, J. Yang, S. Yeganeh, S. R. Yost, I. Y. Zhang, B. R. Brooks, G. K. L. Chan, D. M. Chipman, C. J. Cramer, M. S. Gordon, W. J. Hehre, A. Klamt, H. F. Schaefer, M. W. Schmidt, D. G. Truhlar, X. Xu, A. T. Bell, N. A. Besley, B. D. Dunietz, J. Kong, D. S. Lambrecht, W. Liang, C. Ochsenfeld, L. V. Slipchenko, J. E. Subotnik, T. Van Voorhis, J. M. Herbert, A. I. Krylov and P. M. W. Gill, *Mol. Phys.,* 2015, **113**, 184-215.

11 M. J. Frisch, G. W. Trucks, H. B. Schlegel, G. E. Scuseria, M. A. Robb, J. R. Cheeseman, G. Scalmani, V. Barone, G. A. Petersson, H. Nakatsuji, X. Li, M. Caricato, A. V. Marenich, J. Bloino, B. G. Janesko, R. Gomperts, B. Mennucci, H. P. Hratchian, J. V. Ortiz, A. F. Izmaylov, J. L. Sonnenberg, D. Williams-Young, F. Ding, F. Lipparini, F. Egidi, J. Goings, B. Peng, A. Petrone, T. Henderson, D. Ranasinghe, V. G. Zakrzewski, J. Gao, N. Rega, G. Zheng, W. Liang, M. Hada, M. Ehara, K. Toyota, R. Fukuda, J. Hasegawa, M. Ishida, T. Nakajima, Y. Honda, O. Kitao, H. Nakai, T. Vreven, K. Throssell, J. A. Montgomery, Jr., J. E. Peralta, F. Ogliaro, M. J. Bearpark, J. J. Heyd, E. N. Brothers, K. N. Kudin, V. N. Staroverov, T. A. Keith, R. Kobayashi, J. Normand, K. Raghavachari, A. P. Rendell, J. C. Burant, S. S. Iyengar, J. Tomasi, M. Cossi, J. M. Millam, M. Klene, C. Adamo, R. Cammi, J. W.

Ochterski, R. L. Martin, K. Morokuma, O. Farkas, J. B. Foresman, D. J. Fox, Gaussian 16, Revision C.01; Gaussian, Inc., Wallingford CT, 2019.

12 W. Humphrey, A. Dalke and K. Schulten, *J. Mol. Graph.,* 1996, **14**, 33-38.